GEOPHYSICS. VOL. 76, NO. 6 (NOVEMBER-DECEMBER 2011); P. WC117–WC126, 15 FIGS., 3 TABLES.
10.1190/GEO2011-0028.1

Feasibility of estimating vertical transverse isotropy from microseismic data recorded by surface monitoring arrays

Davide Gei[1], Leo Eisner[2], and Peter Suhadolc[3]

ABSTRACT

Microseismic data recorded by surface monitoring arrays can be used to estimate the effective anisotropy of the overburden and reservoir. In this study we used the inversion of picked P-wave arrival times to estimate the Thomsen parameter δ and the anellipticity coefficient η. This inversion employs an analytic equation of P-wave traveltimes as a function of offset in homogeneous, transversely isotropic media with a vertical axis of symmetry. We considered a star-like distribution of receivers and, for this geometry, we analyzed the sensitivity of the inversion method to picking noise and to uncertainties in the P-wave vertical velocity and source depth. Long offsets, as well as a high number of receivers per line, improve the estimation of δ and η from noisy arrival times. However, if we do not use the correct value of the P-wave vertical velocity or source depth, the long-offset may increase the inaccuracy in the estimation of the anisotropic parameters. Such inaccuracy cannot be detected from time residuals. We also applied this inversion to field data acquired during the hydraulic fracturing of a gas shale reservoir and compared the results with the anisotropic parameters estimated from synthetic arrival times computed for an isotropic layered medium. The effective anisotropy from the inversion of the field data cannot be explained by layering only and is partially due to the intrinsic anisotropy of the reservoir and/or overburden. This study emphasizes the importance of using accurate values of the vertical velocity and source depth in the P-wave arrival time inversion for estimating anisotropic parameters from passive seismic data.

INTRODUCTION

Elastic media, for which seismic velocities depend on the direction of wave propagation, are called anisotropic (Thomsen, 1986). Most crustal rocks are found experimentally to be anisotropic. Anisotropy in sedimentary rock sequences may be caused by the preferred orientation of anisotropic mineral grains (such as in a massive shale formation), the preferred orientation of the shapes of isotropic minerals (such as flat-lying platelets), or the preferred orientation of cracks or thin bedding of isotropic or anisotropic layers (Thomsen, 1986). A transversely isotropic medium with vertical axis of symmetry (VTI) is believed to be the most common anisotropic model for sedimentary basins (Grechka et al., 2002). In this study we consider homogeneous VTI media, which are equivalent (in traveltimes) to complex 1D media of isotropic or VTI layers (Backus, 1962; Grechka and Tsvankin, 1998). We do not use a more complex anisotropy because the observed P-wave arrival times described in the field data section do not seem to require a higher order of symmetry (Eisner et al., 2011).

Ignoring the contribution of the anisotropy to the normal-moveout (NMO) velocity in shale reservoirs leads to misties in time-to-depth conversion (Banik, 1984; Alkhalifah et al., 1996; Sarkar and Tsvankin, 2006). Not only velocity analysis, but practically all other conventional seismic processing and interpretation techniques become inaccurate if the medium is anisotropic (Lynn et al., 1991; Alkhalifah and Larner, 1994; Tsvankin, 1995; Tsvankin and Thomsen, 1995).

A simple methodology of estimating effective anisotropic parameters from long-offset seismic data is the inversion of P-wave arrival times. VTI media are characterized by nonhyperbolic

Manuscript received by the Editor 31 January 2011; revised manuscript received 18 May 2011; published online 30 December 2011; corrected version published online 18 January 2012.
[1]Istituto Nazionale di Oceanografia e di Geofisica Sperimentale (OGS), and University of Trieste, Department of Geosciences, Trieste, Italy. E-mail: dgei@ogs.trieste.it.
[2]Czech Academy of Sciences, Institute of Rock Structure and Mechanics, Prague, Czech Republic. E-mail: leo@irsm.cas.cz.
[3] University of Trieste, Department of Geosciences, Trieste, Italy. E-mail: suhadolc@units.it.

reflection moveouts, which are more significant in large-offset arrivals for P-waves. The nonhyperbolicity of the moveout can also be related to vertical and lateral heterogeneity and reflector curvature (Fomel and Grechka, 1997). This technique, widely used for active seismic prospecting (Tsvankin and Thomsen, 1994; Alkhalifah and Tsvankin, 1995; Grechka and Tsvankin, 1998), can be efficiently applied to microseismic data analysis as well. Although microseismic events also generate split S-waves that provide an evidence of anisotropy (e.g., Verdon et al., 2009), the first arrivals of P-waves can generally be unambiguously picked in noisy (surface) data. Thus, this study will focus on P-waves only.

Anisotropy is routinely inverted from active data through various techniques. The most commonly used configuration is the VSP-type of acquisition (e.g., Jech and Pšenčík, 1992), where receivers are lowered into a borehole and active sources (shots or vibroseis) are located at the surface. In such experiments both receiver position and shot timing are known with sufficient precision. Furthermore, receivers are distributed over some depth interval. In passive seismic geometry, discussed in this study, only one depth interval of calibration shots is usually available, and the timing of the shot is usually unknown. Therefore, this study focuses on the feasibility of this poorer inversion with additional unknowns. Alternatively, the presence of anisotropy can be inferred from the S-wave splitting observed in downhole data (e.g., Verdon et al., 2009). However, we are studying the feasibility of using P-waves only from surface data because they might provide an alternative measurement to S-wave splitting when the S-wave model is not sufficiently known.

Hydraulic fracture stimulation (fracking) is commonly used to enhance hydrocarbon recovery by increasing the reservoir permeability. These stimulations consist of injecting high-pressure fluids into rock formations. Such injections induce microseismic events that are monitored to optimize the hydraulic fracturing. A star-shaped array of surface (or near-surface) geophones can be used to monitor the induced microseismicity. The monitoring of induced seismicity differs from active seismic prospecting by having more unknowns. The origin time is obviously not known for microseismic events and often even for perforation shots. The locations of perforation shots are known with a limited precision, which depends on the accuracy of a well-deviation survey (Bulant et al., 2007). A velocity model is usually calibrated from seismic signals of perforation shots at known positions along the treatment well.

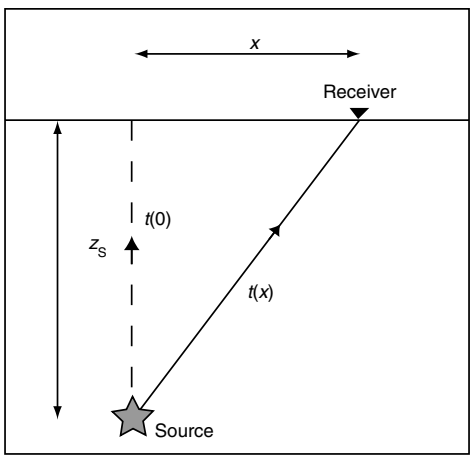

Figure 1. Schematic representation of a passive seismic monitoring experiment.

Chambers et al., (2010b) test the ability to detect microseismic events with a surface star-like array by locating several perforation shots in isotropic layered media. The application of isotropic velocity models to surface monitoring of induced microseismicity is also discussed by Chambers et al. (2010a) in an application of data from Valhall. In their study, the authors used an isotropic model built on active seismic monitoring, whereas this study investigates the possibility of building an effective anisotropic model.

In this study, we investigate the feasibility of inverting passive seismic data for effective anisotropic parameters, assuming a VTI model of the subsurface. We investigate the sensitivity of the P-wave arrival time inversion to picking errors and uncertainties in the P-wave vertical velocity and source location. We also aim to better understand the effects of the possible incorrectness of these input parameters on the results of the inversion and to verify the effectiveness and limits of using large offsets and short receiver spacing. Moreover, we show some results of the application of the P-wave arrival time inversion to four perforation shots at a gas shale reservoir as an example of practical velocity model calibration.

We use star-array geometry for our synthetic tests as this layout is similar to the field test of this study. We believe our conclusions are not significantly affected by the chosen geometry, as illustrated by Zhang et al. (2011) (Zhang, Y., L. Eisner, W. Barker, M. C. Mueller, K. Smith, 2011, Consistent imaging of hydraulic fracture treatments from permanent arrays through calibrated velocity model: submitted to Geophysical Prospecting).

P-WAVE TRAVELTIME INVERSION FOR HOMOGENEOUS TRANSVERSELY ISOTROPIC (TI) MEDIA

Traditionally, the inversion of P-wave traveltime has been used for active seismic applications (Tsvankin and Thomsen, 1994; Alkhalifah and Tsvankin, 1995; Grechka and Tsvankin, 1998). Considering a straight-line raypath in a single horizontal homogeneous isotropic layer, the traveltime of the direct P-wave from a subsurface source is given by

$$t(x)^2 = t(0)^2 + x^2/{V_{\mathrm{NMO}}}^2, \tag{1}$$

where $t(0)$ is the zero-offset one-way traveltime, x is the offset, i.e., the horizontal distance from the source, and V_{NMO} is the normal-moveout velocity, being the P-wave velocity of the isotropic medium (Figure 1). The moveout travel-time described by equation 1 is hyperbolic.

Let us consider a single horizontal homogeneous transversely isotropic layer with a vertical symmetry axis (VTI). In the small offset approximation equation 1 still holds, but

$$V_{\mathrm{NMO}} = V_{\mathrm{P0}}(1+2\delta)^{1/2}, \tag{2}$$

where V_{P0} is the P-wave vertical velocity and δ is one of the Thomsen parameters (Thomsen, 1986). In small offsets the moveout is still hyperbolic, but V_{NMO} is neither the vertical, nor the horizontal P-wave velocity of the medium.

Alkhalifah and Tsvankin (1995) showed that, in laterally homogeneous VTI media, the traveltimes of qP-waves depend mainly on the zero-dip normal-moveout velocity V_{NMO} and the anellipticity parameter η, controlling the nonhyperbolic moveout:

$$\eta = \frac{\epsilon - \delta}{1 + 2\delta}, \tag{3}$$

where ϵ is one of the Thomsen parameters, whose value in VTI media is close to the fractional difference between the horizontal and vertical P-wave velocities (Thomsen, 1986).

Alkhalifah and Tsvankin (1995) modified a three-term Taylor series expansion of the moveout given by Tsvankin and Thomsen (1994) as

$$t^2(x) = t^2(0) + \frac{x^2}{V_{\mathrm{NMO}}^2} - \frac{2\eta x^4}{V_{\mathrm{NMO}}^2[t^2(0)V_{\mathrm{NMO}}^2 + (1+2\eta)x^2]}, \tag{4}$$

where V_{NMO} is given by equation 2. Here the coefficient of x^4 is modified to fit the horizontal velocity. This moveout equation is suitable for computation of P-wave traveltimes in the large-offset approximation. Furthermore, the equation holds even for computing the traveltime from a source at depth to the surface, if x is the horizontal distance of the receiver from the source and $t(0)$ is the one-way traveltime. This equation can be used to invert arrival times from microseismic events or perforation or calibration shots. Arrival times can be inverted in a nonlinear iterative inversion minimizing the residuals between observed and synthetic traveltimes. This inversion uses as input arrival times $t_{\mathrm{A}}(x)$ determined along various offsets. The traveltimes $t(x)$ in equation 4 are matched with the arrival times corrected for an origin time t_0 as

$$t(x) = t_{\mathrm{A}}(x) - t_0. \tag{5}$$

Thus, to invert VTI parameters δ and η, we need to either know or invert origin time t_0, vertical P-wave velocity V_{P0}, the depth of the source, and the one-way vertical traveltime $t(0)$). Without restriction to generality, we assume that the horizontal position of the source is either known with sufficient accuracy (perforation shots) or determined from symmetry of the moveout, independently of the velocity model calibration.

SYNTHETIC DATA

In this section we describe the synthetic data set, which is similar to the real data sets discussed in the field data section. Here we investigate synthetic arrival times for homogeneous anisotropic media equivalent to a layered model with a vertical axis of symmetry; such a model is appropriate for most fractured shale basins. Figure 1 shows a vertical cross section through the synthetic passive seismic monitoring experiment of this study. The microseismic source is located at depth z_S and the receiver at offset x; $t(x)$ is the traveltime at offset x and $t(0)$ is the one-way vertical traveltime. To compute synthetic arrival times and perform the P-wave arrival time inversion, receivers are arranged in eight regularly spaced lines (45° spacing) radiating from a central point, in a star-like pattern. The source is located in the center of the star at a depth of 2100 m, as illustrated in Figure 2. The coordinates of the source are $x_{\mathrm{S}} = 3350$ m, $y_{\mathrm{S}} = 3350$ m, and $z_{\mathrm{S}} = 2100$ m. The effective vertical velocity $V_{\mathrm{P0}}^{\mathrm{true}}$ is 2906 m/s and the anisotropic parameters are $\delta = 0.1$ and $\eta = 0.1$. We chose δ to be equal to η, as we want to compare the relative changes of these parameters in the inversion. From the computed traveltimes we subtract 0.5 s, corresponding to the origin time $t_0 = -0.5$ s.

The traveltimes are computed using equation 4, i.e., we use the same equation for forward and inverse modeling. We have also used alternative computations of traveltimes (e.g., traveltimes computed with equations listed in Bulant et al. (2007) and full-wave numerical modeling (Carcione, 2007) and picking) and have obtained similar results. Therefore, we assume that this choice does not affect our conclusions. To simulate picking noise, we perturb synthetic arrival times with Gaussian noise with zero mean and increasing values of standard deviation σ_n, from 0 to 4 ms. The standard deviation of the Gaussian noise is given by

$$\sigma_n = \sqrt{\frac{\sum_{i=1}^{N} n_i^2}{N}}, \tag{6}$$

where n_i is the noise added to the arrival times and N is the number of arrival times in the data set. And analogously the rms of residuals, either from synthetic or real data sets, is

$$\mathrm{rms} = \sqrt{\frac{\sum_{i=1}^{N} (t_i^{\mathrm{data}} - t_i^{\mathrm{synth}})^2}{N}}, \tag{7}$$

where t_i^{data} are input arrival times and t_i^{synth} are computed arrival times.

SENSITIVITY ANALYSIS OF P-WAVE TRAVELTIME INVERSION

In the following inversion tests we invert for anisotropic parameters δ and η and origin time t_0. For input parameters we use arrival times with variable noise levels, the vertical P-wave velocity V_{P0}, and the source location (x_{S}, y_{S}, z_{S}). We investigate the sensitivity of the inverted parameters to input parameters, particularly the source depth and vertical P-wave velocity. We consider the horizontal coordinates of the source (x_{S} and y_{S}) as known parameters, as they can be robustly inverted in VTI media. We do not invert more

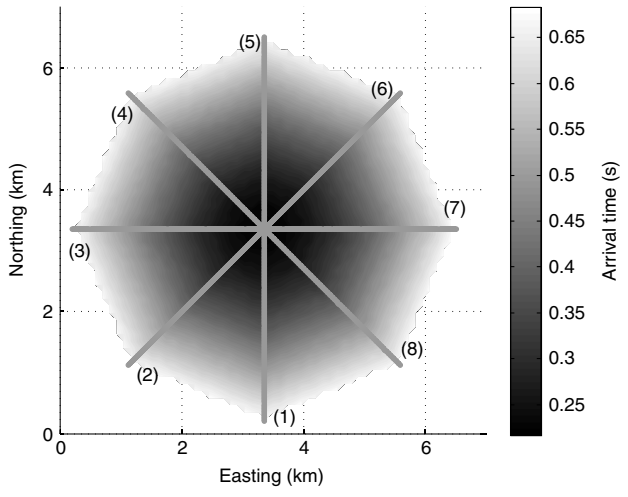

Figure 2. Arrival time contour over a plan view of a typical layout for surface array monitoring of hydraulic stimulations. The source is located in the center of the star. The gray lines represent the different arms of the star-pattern array.

than three parameters (δ, η, and t_0) because equation 4 shows that only three coefficients of the Taylor expansion can be determined independently. This is analogous to the inversion described in Bulant et al. (2007), in which only three parameters were determined independently. In our case, we chose the origin time and anisotropy as unknowns. However, if the origin time is known we can invert for the vertical velocity instead.

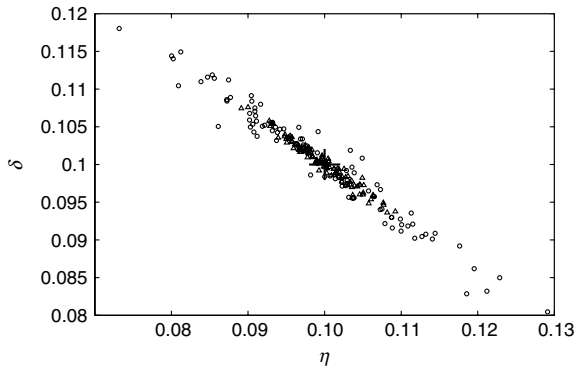

Figure 3. Anisotropic parameters δ versus η as results of inversions of traveltimes perturbed with 100 different realizations of Gaussian noise ($\sigma_n = 4$ ms). Triangles correspond to inversions with the star geometry and circles indicate inversions with a single-line geometry. The cross indicates the actual values of the anisotropic parameters ($\delta = 0.1$ and $\eta = 0.1$).

Sensitivity to picking noise

In principle, once the VTI character of the subsoil has been ascertained, the inversion of P-wave arrival times can be performed for a single seismic line, e.g., a single arm of the star-array. However, in the presence of picking noise, a large number of arrival times given by an equally large number of receivers provides better statistical sampling resulting in a more precise estimate of anisotropic parameters δ and η. Figure 3 shows the results of 100 inversions, each of them characterized by a different realization of the Gaussian noise ($\sigma_n = 4$ ms). The maximum offset-to-source-depth ratio (MO/SD) is 1.5, the receivers spacing is 16 m, and the number of receivers per line is 200. Triangles and circles show inverted δ and η using the eight-arm star-array and line 1 alone, respectively. The two anisotropic parameters are characterized by a linear trend as values of δ and η trade off with one another. Inversions of the data set from the star-array result in tighter clustering than inversions of the data from single line 1, both centered on the true (input) values. All inversions in this study are performed using the star-array geometry.

Figure 4a and b shows δ and η, respectively, inverted from synthetic arrival times perturbed with different levels of Gaussian noise σ_n. Figure 4c and d shows inverted origin times t_0 and the root mean square of time residuals (rms). The maximum offset-to-source-depth ratio (MO/SD) is 1.5, the receiver spacing is 16 m, and the number of receivers per line is 200. For each noise level (σ_n) we compute 100 realizations. Inaccuracies in the estimated anisotropic parameters are proportional to the picking noise, and η is more sensitive than δ to the noise level. t_0 is little affected by the picking noise. The rms of time residuals (Figure 4d) has the same value of σ_n; thus, we may use the measured rms values in a real data set as an estimate of the noise in picked arrival times.

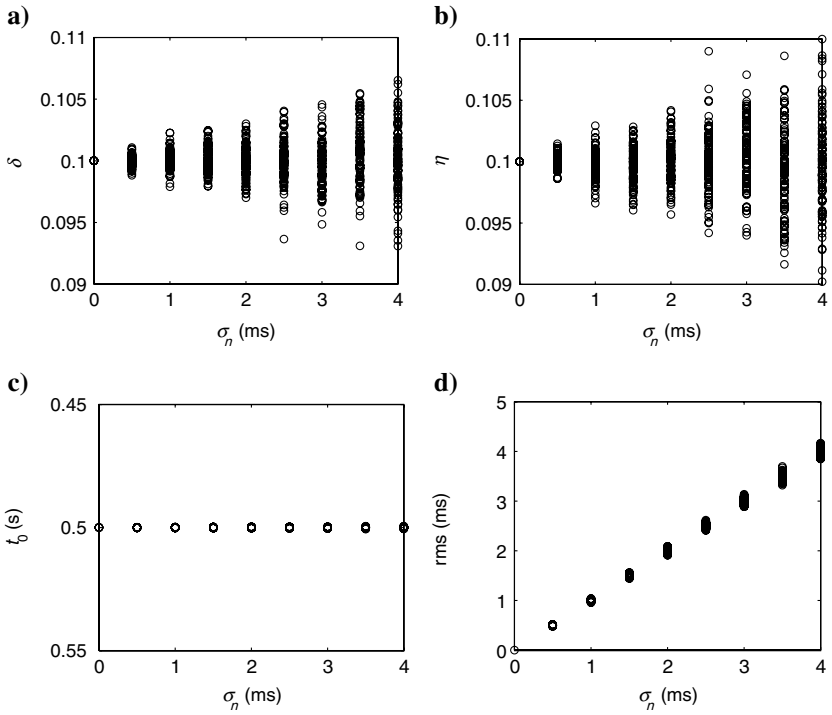

Figure 4. Estimated anisotropic parameter δ (a), η (b), origin time t_0 (c), and rms of time residuals (d) for nine values of the standard deviation of Gaussian noise (σ_n). The maximum offset-to-source depth ratio (MO/SD) is 1.5, the receiver spacing is 16 m, and the number of receivers per line is 200.

Figure 5a and b shows the standard deviation of δ and η, respectively, versus the MO/SD with σ_n of 4 ms. For each MO/SD value, the curves represent the standard deviation of 100 estimated anisotropic parameters, corresponding to 100 noise realizations in the synthetic arrival-times. Figure 5 shows three curves in each plot. To obtain the curves defined by circles, we increase the offset by adding receivers to each arm of the star-array; the receiver spacing is constant (25 m) and the number of receivers varies between 63 (MO/SD = 0.75) and 168 (MO/SD = 2). The curves defined by asterisks are computed by keeping constant the number of receivers per line (100) and increasing the receiver spacing from 16 m (MO/SD = 0.75) to 42 m (MO/SD = 2). The curves given by triangles use 200 receivers per line and receiver spacing from 8 m (MO/SD = 0.75) to 21 m (MO/SD = 2). The standard deviation of the inverted δ and η decreases as MO/SD increases. The fastest decrease of the error is for MO/SD smaller than one, and the improvement to the inverted anisotropic parameters from offsets larger than 1.5 source depth is negligible. A greater number of receivers per line provides a better estimate of anisotropic parameters by means of

a better statistical sampling of noise. This conclusion is similar to the one obtained with the test in Figure 3. Increasing the maximum offset by adding receivers to the seismic lines results in the most effective reduction of the standard deviations of δ and η.

This is also shown in Figure 6a and b by plotting the standard deviation of δ and η, respectively, as a function of the number of receivers per line (nr) for a fixed MO/SD. For each value nr we show the standard deviations of δ and η, resulting from 100 noise realization of arrival times. MO/SD is 1.5 and the arrival times are affected by the picking noise with the σ_n of the normal distribution of 4 ms. The maximum offset is kept constant, and increasing the number of receivers reduces the receiver spacing. The estimated values of δ and η dramatically improve as more receivers are added to each arm of the star-array: up to 200 receivers corresponding to a receiver spacing of 15 m. Note that the uncertainty reduction falls off approximately as $\frac{1}{\sqrt{N}}$, where N is the number of receivers.

Sensitivity to P-wave vertical velocity

To study the sensitivity of this P-wave arrival time inversion technique to the input value of the P-wave velocity in the vertical direction (V_{P0}) we perform arrival-time inversions considering seven different velocity values, ranging from -10% to $+10\%$ of the actual value $V_{P0}^{true} = 2960$ m/s. Synthetic traveltimes are computed with the actual values of the P-wave vertical velocity V_{P0}^{true}, but they are inverted in view of the incorrect values of V_{P0}.

Figure 7 shows the inverted δ, η, origin time t_0, and the rms of the time residuals, respectively, as a function of the assumed input P-wave vertical velocity V_{P0}. For each value of the P-wave vertical velocity, we perform 100 inversions, corresponding to 100 noise realizations in the synthetic arrival-times. The standard deviation of the Gaussian noise is 4 ms. The maximum offset-to-source-depth ratio is 1.5 and the number of receivers per arm is 200. Each circle in Figures 7a–d represents the result of one of the 100 performed inversions. For P-wave vertical velocities differing from the actual value V_{P0}^{true}, the estimated δ (Figure 7a) and η (Figure 7b) reveal a systematic bias increasing almost linearly with the actual difference between the correct and input vertical velocity. However, the scatter (or standard deviation) of the inverted anisotropic parameters remains approximately constant and depends on the level of noise in the arrival-times (Figure 7d). The bias, or accuracy, of the two inverted anisotropic parameters is proportional to $|V_{P0} - V_{P0}^{true}|$. The scatter, or precision, depends only on the level of noise in the arrival times. Because the noise level was kept constant in this test, the inverted δ and η show a constant scatter for all the V_{P0} values. Origin time t_0, shown in Figure 7c, is not affected by the Gaussian noise but depends on the input P-wave vertical velocity. The rms of the time residuals (Figure 7d) equals the noise level (σ_n) but is unaffected by V_{P0}. The presence of picking noise in the input arrival times can be inferred from the root mean square of the time residuals. Instead, inaccurate values of the input P-wave vertical velocity cause proportional inaccuracies in the estimated anisotropic parameters that cannot be detected from the rms or any other result of the inversion.

Figure 8a and b shows the dependence of the means (solid lines) and standard deviations (shaded areas) of 100 inverted δ and η on the maximum offset-to-source-depth ratio (MO/SD). We show three dependences for three different input vertical velocities: $V_{P0} = 0.9V_{P0}^{true}$, $V_{P0} = V_{P0}^{true}$, and $V_{P0} = 1.1V_{P0}^{true}$. The input arrival times are perturbed with Gaussian noise ($\sigma_n = 4$ ms). The symbols in Figure 8a and b are the mean values of the anisotropic parameters inverted from 100 realizations of randomly distributed Gaussian noise in the synthetic arrival times. They represent the accuracy of the inversion method as a function of MO/SD and V_{P0}. The standard deviations σ_δ and σ_η (shaded area) for the increasing maximum

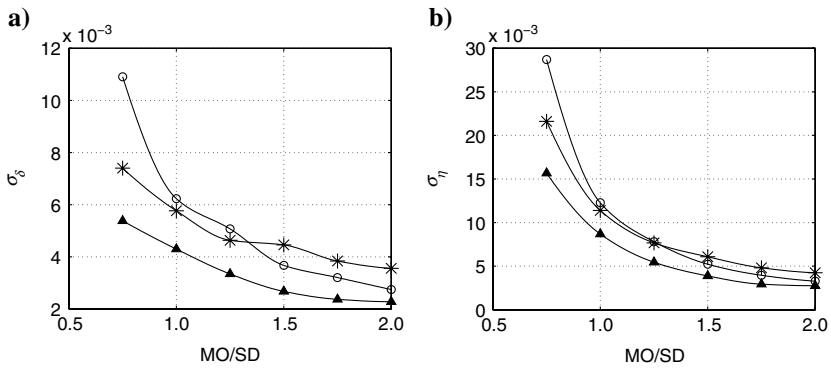

Figure 5. Standard deviation of 100 estimations of anisotropic parameters δ (a) and η (b) versus maximum offset-to-source-depth ratio (MO/SD). The standard deviation for the Gaussian noise perturbing the synthetic traveltimes is 4 ms. For curves defined by circles, the maximum offset is increased by increasing the number of receivers in each line of the star-array from 63 (MO/SD = 0.75) to 168 (MO/SD = 2). For curves, given by asterisks and triangles, the arms are stretched, increasing the receiver spacing with a constant number of receivers per line of 100 and 200, respectively.

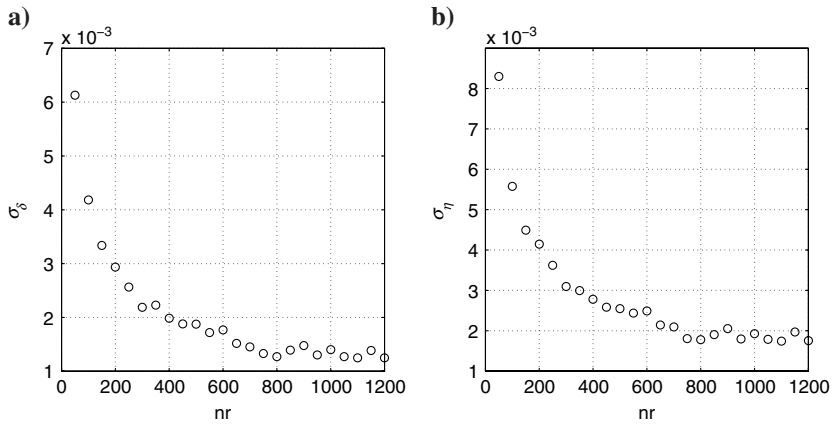

Figure 6. The standard deviation of anisotropic parameter δ (a) and anellipticity coefficient η (b) versus the number of receivers per line (nr). Each circle is the standard deviation of 100 estimations corresponding to the same number of different noise realizations. The maximum offset-to-source-depth ratio is 1.5. The standard deviation for the Gaussian noise is 4 ms.

offset-to-source-depth ratio are related to the Gaussian noise in the arrival times. The surprising result is increasing bias (inaccuracy) for η with increasing maximum offset for $V_{P0} \neq V_{P0}^{true}$. There are two sources of uncertainty in the estimated parameters: the lack of accuracy, highlighted by the means and related to the incorrect value of V_{P0}, and the lack of precision, highlighted by the standard deviations and due to the picking noise. For the Thomsen parameter δ, both the accuracy and precision improve with increasing MO/SD.

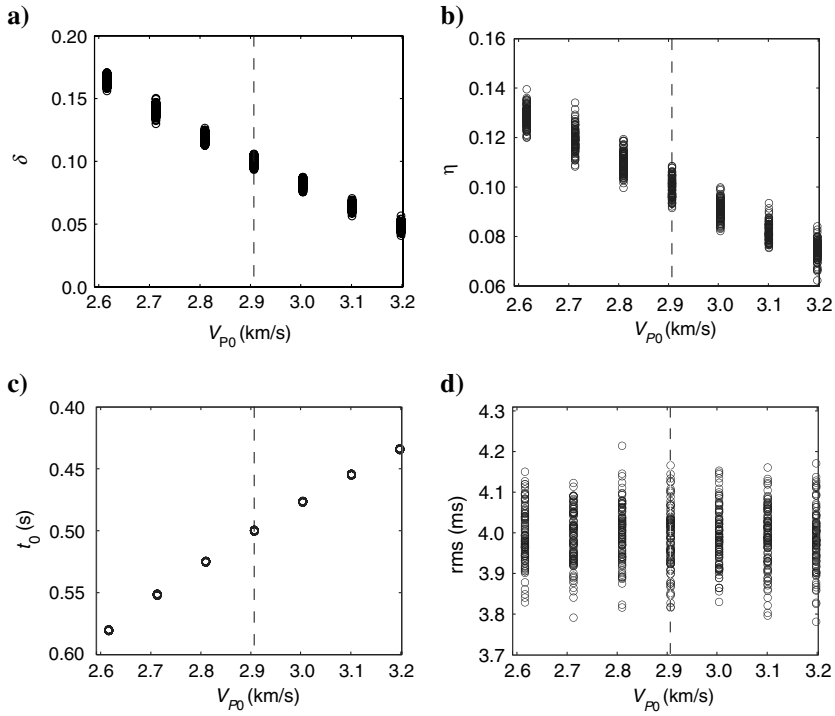

Figure 7. Anisotropic parameter δ (a), η (b), origin time t_0 (c), and rms of time residuals (d) versus P-wave vertical velocity. The maximum offset-to-source-depth ratio is 1.5, the standard deviation for Gaussian noise is 4 ms, and the number of receivers per line of the star-array is 200. The vertical dashed lines represent the true velocity value.

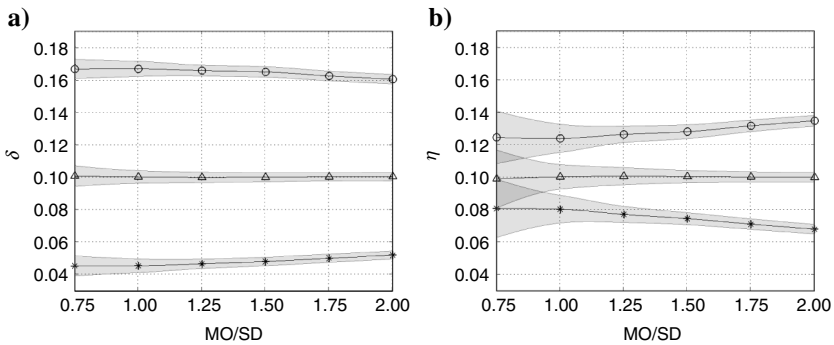

Figure 8. The means (solid lines) and standard deviations (shaded areas) of δ (a) and η (b) versus offset-to-source-depth ratio (MO/SD). We use $V_{P0} = 0.9V_{P0}^{true}$ for data points represented by circles, $V_{P0} = V_{P0}^{true}$ for triangles and $V_{P0} = 1.1V_{P0}^{true}$ for asterisks. The standard deviation for Gaussian noise is 4 ms. The means and standard deviations are computed from the results of 100 inversions corresponding to the same number of noise realizations.

The accuracy of the anellipticity coefficient η strongly decreases as the maximum offset increases, and the precision slightly increases.

Sensitivity to source depth

Similar to the test used for the sensitivity analysis to the P-wave vertical velocity, we invert the arrival times perturbed with white Gaussian noise ($\sigma_n = 4$ ms) with various source depth values z_S' ranging from $0.95z_S$ to $1.05z_S$, where $z_S = 2100$ m is the actual source depth used to compute the arrival times.

Figure 9 shows δ, η, origin time t_0, and the rms of the time residuals, respectively, as a function of z_S'. For each value z_S' we perform 100 inversions, corresponding to 100 noise realizations. The standard deviation of the Gaussian noise is 4 ms. The maximum offset to the source depth ratio is 1.5, and the number of receivers in each line is 200. For source depths different from the actual value, the inverted δ and η are characterized by a systematic error proportional to $|z_S' - z_S|$. The depth z_S' affects the accuracy, but not the precision, of the inversion results. The precision is again controlled by noise in the arrival times only, because the scatter remains constant in Figure 9a, b, and d. The inverted origin times (Figure 9c) are not affected by the Gaussian noise, but they strongly depend on the source depth.

Figure 10a and b shows the means (solid lines) and standard deviations (shaded areas) of δ and η as a function of the source-to-depth ratio (MO/SD); three values of source depths were tested: $z_S' = 0.95z_S$, $z_S' = z_S$, and $z_S' = 1.05z_S$. The accuracy of the inversion of both anisotropic parameters decreases with increasing offset. This can be understood from the fact that the VTI anisotropy mainly affects horizontal traveltimes. Thus, as the offset increases, the raypaths become more horizontal, and the erroneous depth is compensated by larger values of the VTI parameters. The precision of the inversion method, emphasized by standard deviations σ_δ and σ_η, strongly increases with MO/SD. The increasing of the precision, inferred by the narrowing of the shaded areas with increasing MO/SD, could give an incorrect impression of obtaining more accurate results. Similar to the results of the P-wave vertical velocity test, the noise level in the arrival times can be gathered from the rms of the time residuals. An incorrect source depth causes inaccuracies in the estimated δ and η, and this inaccuracy increases with greater maximum offsets. Such inaccuracies do not occur with any output parameter of the inversion.

The results of testing the P-wave arrival time inversion with synthetic traveltimes are summarized in Table 1. Uncertainties in the input parameters are given in roman type and their effect on the results of the inversions are given in italic type.

FIELD DATA

Microseismic monitoring was performed by Microseismic Inc. during the hydraulic fracturing of a gas shale reservoir located in North America and operated by Newfield Exploration Mid-Continent Inc. They used a 10-line Fracstar® array (Figure 11) with 1C geophones located on the earth's surface. The number of receivers per arm varied between 54 (line four) and 122 (lines two and 10) and the average receiver distance was 23 m. The formation was accessed by perforating the casing at reservoir depth. Such perforation shots are generally used to calibrate the velocity model in downhole and surface monitoring. As the tests on synthetic data sets in previous sections revealed, the inverted anisotropic parameters depend on the correct depth of the microseismic event. The depth of induced microseismic events is unknown; therefore, the inversion was performed from perforation shots, whose positions are known with high accuracy (less than 2% error, as discussed in Bulant et al., 2007). We apply the previously described inversion to P-wave arrival times measured from perforation shots. All of the shots belong to the same stage with a horizontal shot separation of 37 m; the vertical separation of shots is negligible. Perforation shot coordinates are given in Table 2.

Figure 11 shows the manually picked and interpolated arrival times for perforation shot 1. Microseismic data from the northwestern part of the array are too noisy to pick the first arrivals.

Figure 12 shows an example of seismic sections relative to shot 1. We apply a band-pass frequency filter with corner frequencies 6, 12, 60, and 70 Hz.

To apply the P-wave traveltime inversion for homogenous-anisotropic media to this data set, we compute the effective vertical velocity at the source depth: for a given depth of a seismic source, the effective velocity is the P-wave velocity of an equivalent homogeneous medium yielding the same zero-offset travel-time as the layered medium. Figure 13 shows the 1D P-wave vertical velocity profile derived from 3D active seismic over the reservoir (continuous lines) and the effective vertical velocity (dashed curve). The effective velocity at the depth of the perforation shots is $V_{P0} = 2906$ m/s.

Figure 14a and b shows the time residuals of perforation shot 1 interpolated in a map-view plot and as a function of offset, respectively. The results of the inversions of picked arrival times from the four perforation shots are given in Table 3. δ and η are high, indicating an anisotropic medium. The anisotropic parameters shown in Table 3 are similar from shot to shot, although they were obtained from independently picked arrival times of the four perforation shots. Shot 4 yields a slightly higher δ and a lower η than the other shots. Because of the strong noise level in the northwestern part of the array, we could pick only arrivals from lines (1), (2), (3), (10), and part of (9) (see Figure 11 for line number reference). This makes shot 4 the least constrained. Finally, the resulting rms is comparable to the test of Figure 3; we can see that the scatter of the inverted anisotropic parameters is very consistent, and even the "error" of inverted parameters from shot 4 is consistent with the δ-η trade-off observed in the test on the synthetic data set.

The nonhyperbolicity of the moveout can also be caused by vertical and lateral heterogeneity (Backus, 1962; Fomel and Grechka,

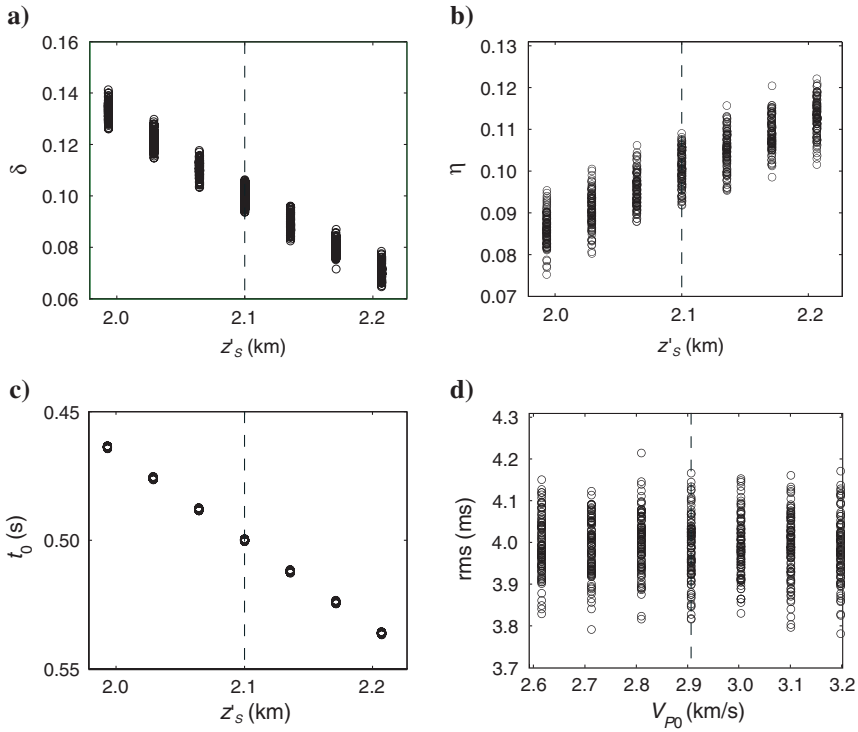

Figure 9. Anisotropic parameter δ (a), η (b), origin time t_0 (c), and the rms of the time residuals (d) versus source depth. The maximum offset-to-source-depth ratio is 1.5, the standard deviation for Gaussian noise is 4 ms, and the number of receivers per line of the star-array is 200. The vertical dashed lines represent the true source depth value.

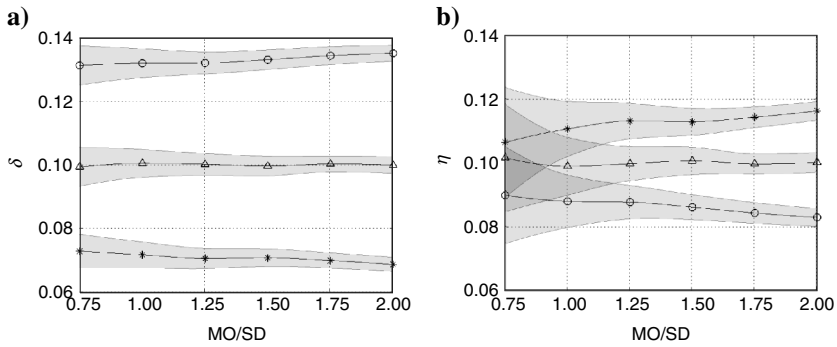

Figure 10. The means (solid lines) and standard deviations (shaded area) of δ (a) and η (b) versus the offset-to-source-depth ratio (MO/SD). We use $z'_S = 0.95z_S$ for data points represented by circles, $z'_S = z_S$ for triangles, and $z'_S = 1.05z_S$ for asterisks. The standard deviation for Gaussian noise is 4 ms. The means and standard deviations are computed from the results of 100 inversions corresponding to the same number of noise realizations.

1997). Inversions of arrival times in isotropic layered media can result in apparent anisotropy. To estimate the influence of layering on the above inverted effective anisotropy we compute and invert synthetic arrival times for a layered isotropic medium. We consider a horizontally layered model suitable for this data set with the P-wave velocity profile shown in Figure 13 (continuous line).

Table 1. Summary of the results of P-wave arrival time inversions of synthetic data.

Picking noise		δ	η	t_0
		*Scattered**†	*Scattered**†	*No effect*
Velocity	Lower than V_{P0}^{true}	*Higher**	*Higher*	*Lower*
	Higher than V_{P0}^{true}	*Lower**	*Lower*	*Higher*
Source depth	Lower than z_S	*Higher*	*Lower*	*Higher*
	Higher than z_S	*Lower*	*Higher*	*Lower*

*Long offsets improve the estimation.
†A high number of receivers per line improves the estimation.

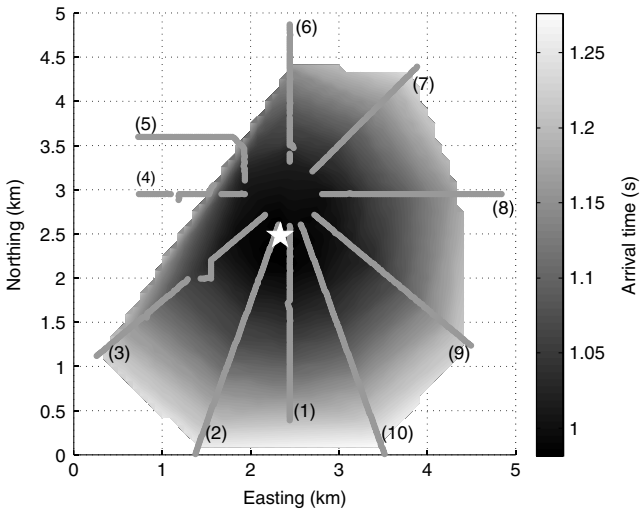

Figure 11. A contour plot showing the picked arrival times for perforation shot 1. The straight, gray, numbered lines represent the 10 seismic lines of the Fracstar. The white star is the source location.

Table 2. Input parameters for P-wave arrival time inversions of field data.

	Easting (m)	Northing (m)	Depth (m)	V_{P0}^{true} (m/s)
Shot 1	2343	2410	2100	2906
Shot 2	2341	2517	2100	2906
Shot 3	2341	2552	2099	2906
Shot 4	2342	2590	2100	2906

We compute the synthetic traveltimes in the isotropic layered model and add Gaussian noise with zero mean and $\sigma_n = 4$ ms, similar to the residuals observed in the inversions of the field data. Figure 15 shows the time residuals from the inversion of synthetic arrival times computed with the same geometry of the field data (see Figure 14). Table 2 shows the inverted anisotropic parameters, which are only about 50% of the anisotropic parameters observed in the inversion of the real data set, assuming a homogeneous medium. Hence, we conclude that the isotropic layers seem to cause only about 50% of the effective anisotropy, indicating that the medium is also anisotropic.

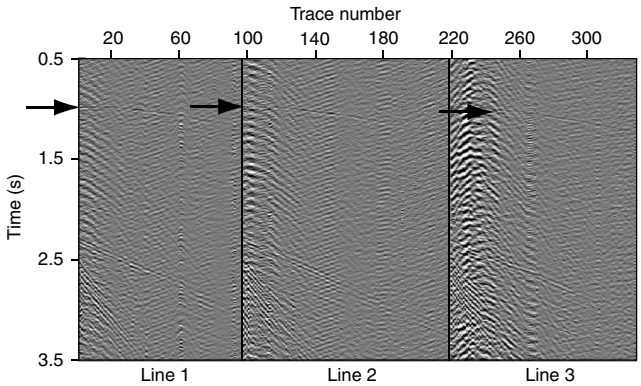

Figure 12. Seismic sections of lines 1–3 for shot 1. The first arrivals are indicated by arrows.

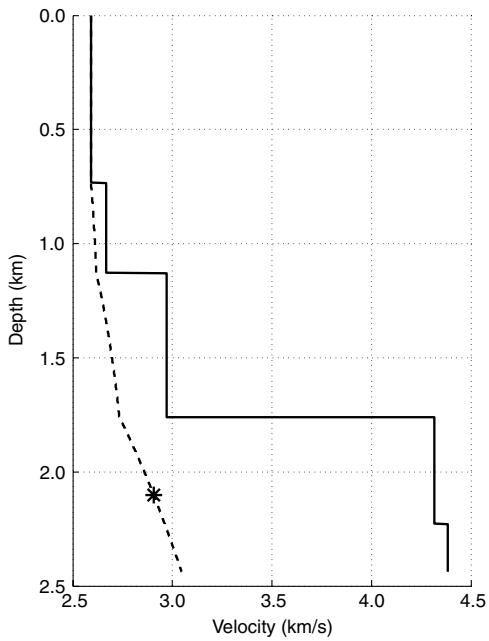

Figure 13. A 1D vertical P-wave velocity profile of the study area. The interval velocity is given by the continuous line and the dashed line is the effective vertical velocity. The asterisk represents the effective velocity ($V_{P0} = 2906$ m/s) with the source located at 2100 m, the depth of the perforation shots.

A more general conclusion about the inverted anisotropic parameters requires the generalization of the methodology to at least 1D layered media. The observed anisotropy strength seems to be consistent with that observed in active seismics. The residuals observed in the test on the real data set are surprisingly low, suggesting small effects of the near-surface structure in this area.

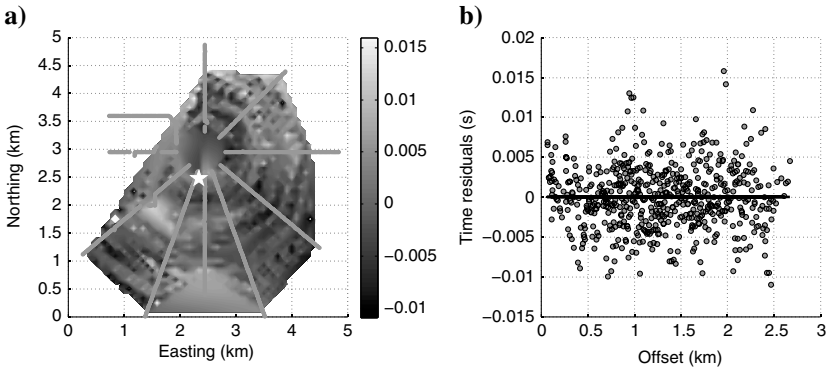

Figure 14. (a) Contour plot showing the time residuals from the inversion of field data (shot 1); the straight gray lines represent the 10 arms of receivers of the Fracstar, and the white star is the source location. (b) The time residuals of perforation shot 1 of picked arrival times versus offset.

Table 3. Results of P-wave arrival time inversions of field data.

	t_0 (s)	δ	η	rms (ms)
Shot 1	−0.256	0.1173	0.2734	4.0
Shot 2	0.666	0.1207	0.2644	3.4
Shot 3	0.433	0.1205	0.2763	3.3
Shot 4	−0.118	0.1358	0.2223	4.4
Isotropic	0.001	0.0115	0.11,537	4.3

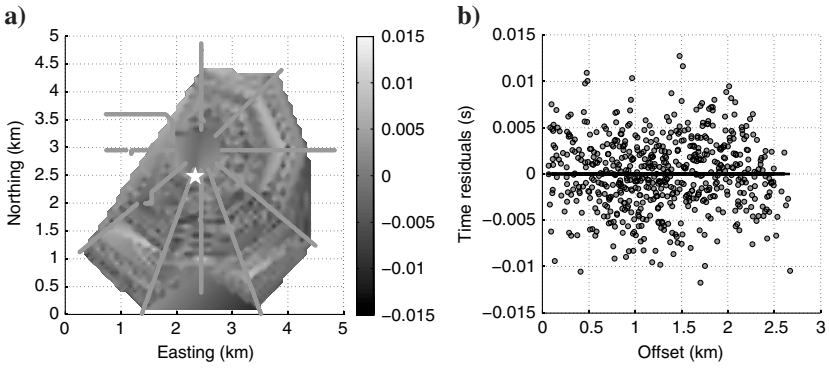

Figure 15. (a) A contour plot showing the time residuals from inversion of synthetic data; the straight, gray lines represent the 10 arms of receivers of the Fracstar, and the white star is the source location. (b) The time residuals of perforation shot 1 of synthetic arrival times versus offset.

CONCLUSIONS

In this study, we investigate reservoir characterization from an array of sensors with a star geometry, deployed on the earth's surface, to monitor hydraulic stimulations. We explore the sensitivity of the P-wave arrival time inversion for homogeneous transversely isotropic media with a vertical axis of symmetry to picking errors and uncertainties in the P-wave vertical velocity and source depth.

The Gaussian noise perturbing the synthetic arrival times affects the precision of the resulting anisotropic parameters δ and η, whereas the origin time is estimated accurately. Long offsets of the lines forming the star-pattern array improve the estimation of anisotropic parameters, most effectively up to 1.5 of the maximum offset-to-depth ratio. Increasing the number of receivers per line of the star-array also increases the precision of the resulting anisotropic parameters, because they improve statistical sampling. Long offsets, and a high number of receivers per line improve the estimation of δ and η from noisy arrival times only if accurate values of the source depth and vertical P-wave velocity are used. If the latter input values are not correctly estimated, the increase of the maximum offset causes a bias of the estimated anisotropic parameters. The precision increases with increasing the length of the maximum offset and the number of receivers, giving an incorrect impression of more accurate results.

Operators and service companies need to use an accurate vertical velocity and good calibration shots to obtain reliable unbiased estimates of anisotropy for microseismic monitoring. A well-calibrated anisotropic velocity model is needed for accurate and unbiased locations of microseismic events.

We also apply the P-wave arrival time inversion to four perforation shots recorded from microseismic monitoring and obtain consistent results from the four independent inversions, resulting in approximately $\delta = 0.27$ and $\eta = 0.12$. Furthermore, we invert the synthetic arrival times computed with an isotropic layered model suitable for this reservoir and obtain an effective anisotropy approximately 50% in strength. Thus, we conclude that the effective anisotropy observed in the field data is caused partially by the intrinsic anisotropic properties of the formations.

ACKNOWLEDGMENTS

We are very grateful to Vladimir Grechka of Shell for guidance, suggestions, and discussions. We are also grateful to the Newfield Exploration Mid-Continent Inc., particularly to Jack Breig, Richard Parkes, Keith Willson, and Michelle Langthorn, for their kind revision, advise, and data. We also thank Microseismic Inc. for the data and support provided for the data management (including the picking software); special thanks are due to Dave Abbott, Michael Thornton, Mike Mueller, Alejandro De La Peña, and Peter Duncan.

REFERENCES

Alkhalifah, T., and K. Larner, 1994, Migration error in transversely isotropic media: Geophysics, **59**, 1405–1418, doi: 10.1190/1.1443698.

Alkhalifah, T., and I. Tsvankin, 1995, Velocity analysis for transversely isotropic media: Geophysics, **60**, 1550–1566, doi: 10.1190/1.1443888.

Alkhalifah, T., I. Tsvankin, K. Larner, and J. Toldi, 1996, Velocity analysis and imaging in transversely isotropic media: Methodology and a case study: The Leading Edge, **15**, 371–378, doi: 10.1190/1.1437345.

Backus, G. E., 1962, Long-wave elastic anisotropy produced by horizontal layering: Journal of Geophysical Research, **67**, 4427–4440, doi: 10.1029/JZ067i011p04427.

Banik, N. C., 1984, Velocity anisotropy of shales and depth estimation in the North Sea Basin: Geophysics, **49**, 1411–1419, doi: 10.1190/1.1441770.

Bulant, P., L. Eisner, I. Pšenčík, and J. L. Calvez, 2007, Importance of borehole deviation surveys for monitoring of hydraulic fracturing treatments: Geophysical Prospecting, **55**, 891–899, doi: 10.1111/gpr.2007.55.issue-6.

Carcione, J. M., 2007, Wave fields in real media: Theory and numerical simulation of wave propagation in anisotropic, anelastic, porous and electromagnetic media: Elsevier Science.

Chambers, K., J. M. Kendall, and O. Barkved, 2010a, Investigation of induced microseismicity at Valhall using the life of field seismic array: The Leading Edge, **29**, 290–295, doi: 10.1190/1.3353725.

Chambers, K., J. M. Kendall, S. Brandsberg-Dahl, and J. Rueda, 2010b, Testing the ability of surface arrays to monitor microseismic activity: Geophysical Prospecting, **58**, 821–830, doi: 10.1111/j.1365-2478.2010.00893.x.

Eisner, L., Y. Zhang, D. Gei, P. Duncan, M. C. Mueller, and M. P. Thornton, 2011, Effective VTI anisotropy for consistent monitoring of microseismic events: The Leading Edge, **30**, 772–776, doi: 10.1190/1.3609092.

Fomel, S., and V. Grechka, 1997, On nonhyperbolic reflection moveout in anisotropic media: Technical Report 92, Stanford Exploration Project, www.sepwww.stanford.edu/public/docs/sep92/sergey4.ps.gz.

Grechka, V., A. Pech, and I. Tsvankin, 2002, P-wave stacking velocity tomography for VTI media: Geophysical Prospecting, **50**, 151–168, doi: 10.1046/j.1365-2478.2002.00307.x.

Grechka, V., and I. Tsvankin, 1998, Feasibility of nonhyperbolic moveout inversion in transversely isotropic media: Geophysics, **63**, 957–969, doi: 10.1190/1.1444407.

Jech, J., and I. Pšenčík, 1992, Kinematic inversion for qP- and qS-waves in inhomogeneous hexagonally symmetric structures: Geophysical Journal International, **108**, 604–612, doi: 10.1111/gji.1992.108.issue-2.

Lynn, W., A. Gonzalez, and S. MacKay, 1991, Where are the fault-plane reflections?: 61st Annual International Meeting, SEG, Expanded Abstracts, 1151–1154.

Sarkar, D., and I. Tsvankin, 2006, Anisotropic migration velocity analysis: Application to a data set from West Africa: Geophysical Prospecting, **54**, 575–587, doi: 10.1111/j.1365-2478.2006.00556.x.

Thomsen, L., 1986, Weak elastic anisotropy: Geophysics, **51**, 1954–1966, doi: 10.1190/1.1442051.

Tsvankin, I., 1995, Normal moveout from dipping reflectors in anisotropic media: Geophysics, **60**, 268–284, doi: 10.1190/1.1443755.

Tsvankin, I., and L. Thomsen, 1994, Nonhyperbolic reflection moveout in anisotropic media: Geophysics, **59**, 1290–1304, doi: 10.1190/1.1443686.

Tsvankin, I., and L. Thomsen, 1995, Inversion of reflection traveltimes for transverse isotropy: Geophysics, **60**, 1095–1107, doi: 10.1190/1.1443838.

Verdon, J. P., J. M. Kendall, and A. Wüstefeld, 2009, Imaging fractures and sedimentary fabrics using shear wave splitting measurements made on passive seismic data: Geophysical Journal International, **179**, 1245–1254, doi: 10.1111/gji.2009.179.issue-2.